ACS Sustainable Chemistry & Engineering
pubs.acs.org/journal/ascecg
Research Article

Insight into the Kinetic Degradation of Stored Nickel-Rich Layered Cathode Materials for Lithium-Ion Batteries

Jiyang Li, Xin Wang, Xiangbang Kong, Huiya Yang, Jing Zeng, and Jinbao Zhao*

Cite This: https://doi.org/10.1021/acssuschemeng.1c02486 Read Online

ACCESS | Metrics & More | Article Recommendations | Supporting Information

ABSTRACT: As the cathode materials for lithium-ion batteries (LIBs), nickel-rich $LiNi_xCo_yMn_{1-x-y}O_2$ (nickel-rich NCM, $0.6 \leq x < 1$) materials have attracted increasing attention. However, during the practical production, transportation, and storage processes, they would suffer from poor storage stability in air, which seriously affects their electrochemical performance. Although researchers have made much effort to understand the degradation mechanism of the storage performance, the relationship between the structural evolution and electrochemical performance degradation still remains ambiguous. In this work, through the detailed structural and electrochemical characterization, the structure−performance relationship of nickel-rich NCM materials during storage in air is established from the aspect of the Li^+ kinetics. It is found that the increased cation mixing would gradually slow down the kinetics of the solid-phase Li^+ diffusion, and the adsorbed species (adsorbed hydroxyl, bicarbonate, carbonated, etc.), impurities (LiOH and Li_2CO_3), and rock salt structure formed on the material surface can significantly weaken the charge transfer kinetics at the electrode/electrolyte interface. In addition, the Li^+ kinetic degradation during charge is much more serious than that during discharge, thereby becoming the dominant factor for the capacity fading during storage. Interestingly, the self-regeneration of the interfacial charge transfer kinetics is found, in which the surface impurities would be decomposed at the end of the first charge (4.0−4.3 V). Therefore, the results obtained in this work is conducive to further understanding the performance degradation mechanism of nickel-rich NCM materials during storage and can provide favorable guidance for the modification research.

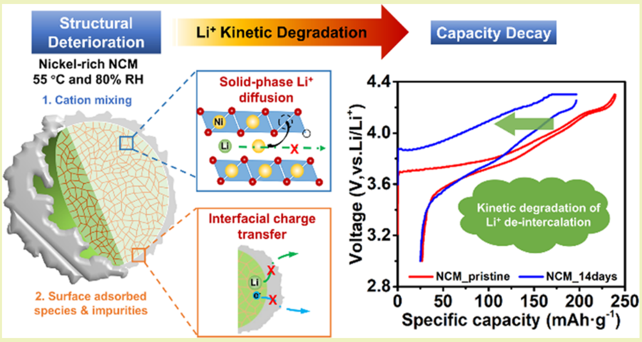

KEYWORDS: *nickel-rich layered cathode, storage, structure−performance relationship, kinetic degradation, Li^+ de/intercalation*

■ INTRODUCTION

In recent years, with the rapid development of the electric vehicle market, the demand for high-energy-density lithium-ion batteries (LIBs) has increased sharply. Owing to the high capacity and the low cobalt content, nickel-rich $LiNi_xCo_yMn_{1-x-y}O_2$ (nickel-rich NCM, $0.6 \leq x < 1$) materials have attracted much attention.[1−5] However, during the practical production, transportation, and storage processes, they would suffer from the poor storage stability in air, which seriously affects their electrochemical performance. For example, the charging voltage plateau gradually increases and the discharging voltage plateau decreases with the storage time, leading to the rapid capacity decay.[6−8]

So far, much effort has been made to understand the structural degradation mechanism of nickel-rich cathode materials during storage, which can be summarized as follows:[7,9−17] (i) The residual alkaline species on the material surface can react with H_2O and CO_2 in air to form surface impurities (LiOH and Li_2CO_3) and adsorbed species (adsorbed hydroxyl, bicarbonate, carbonated, etc.). (ii) The active oxygen species released by the surface spontaneous reduction of Ni^{3+}/Ni^{2+} would react with H_2O and CO_2 in air and further combine with Li^+ to form LiOH and Li_2CO_3. (iii) With the reduction of Ni^{3+}/Ni^{2+} and the extraction of Li^+, a delithiation structure would appear with an increased cation mixing of Li^+/Ni^{2+}. As for the deterioration mechanism of the electrochemical performance during storage, it is generally believed that the surface-adsorbed species and impurities or their reaction products with the electrolyte would isolate the active material particles, hindering the electrical contact and ion transport.[10,13,18,19] All of the abovementioned studies provide valuable information for the comprehensive understanding of the storage performance degradation mechanism of nickel-rich NCM materials. However, the current cognition on the relationship between the structural degradation of the

Received: April 12, 2021
Revised: July 17, 2021

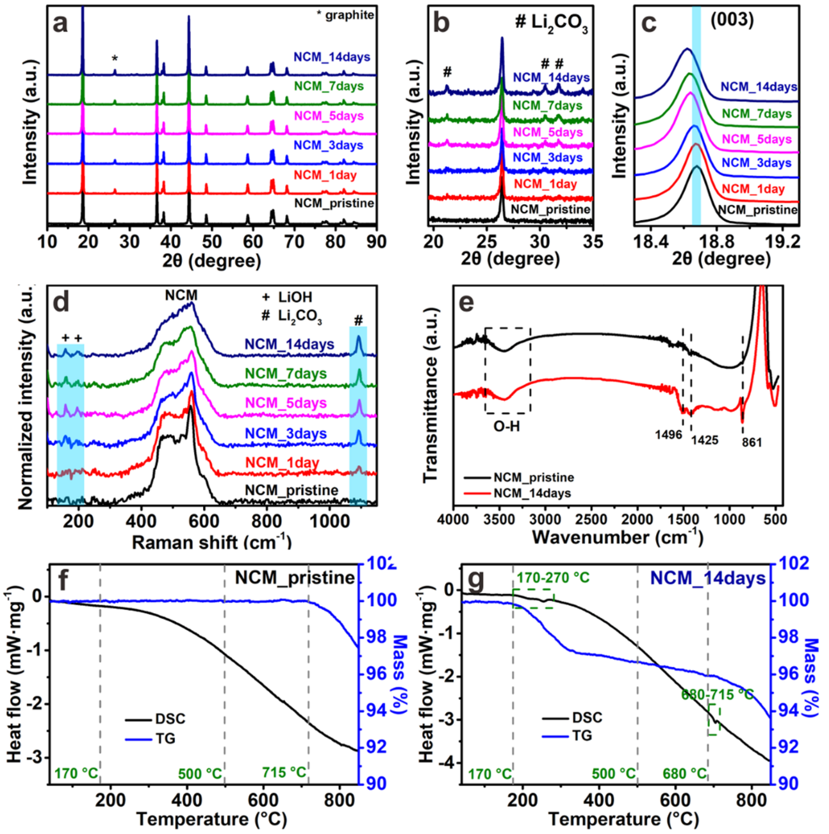

Figure 1. XRD patterns (a−c) and Raman spectra (d) of the nickel-rich NCM materials after being stored for different days. FT-IR spectra (e) and DSC-TG curves (f, g) of the pristine material and the material stored for 14 days.

stored materials and the electrochemical performance deterioration still remains ambiguous, which lacks a more direct connection. In addition, the reaction between the surface impurities (LiOH and Li_2CO_3) and the electrolyte is still controversial. Therefore, it is necessary to systematically investigate the structure−performance relationship of nickel-rich NCM materials during storage.

Recent studies found that the apparent capacity loss of ternary cathode materials during the first cycle mainly originates from the Li^+ kinetic limitation.[20−23] In addition, our previous work also found that the degradation of Li^+ de/intercalation kinetics is responsible for the majority of the capacity loss of the NCM material during cycling at the high-voltage condition.[24] This indicates that the kinetic degradation of Li^+ may be closely related to the electrochemical performance deterioration of the stored nickel-rich NCM materials. Therefore, the purpose of this work is to establish the structure−performance relationship from the aspect of the Li^+ kinetics and deeply understand the kinetic factors leading to the capacity decay during storage.

EXPERIMENTAL SECTION

Storage of Materials. The nickel-rich NCM material used in this work was provided by Beijing Easpring Material Technology Co., Ltd. (China). In order to accelerate the material aging, the storage test was carried out at 55 °C and 80% relative humidity (RH). After being stored for 1, 3, 5, 7, and 14 days, the nickel-rich NCM materials were taken out for further structural and electrochemical measurements.

Structural Characterization. The morphology and element composition of the nickel-rich NCM material were confirmed using a Hitachi TM3030 scanning electron microscope (SEM) and an NCS Plasma-1000 inductively coupled plasma atomic emission spectrometer (ICP-AES). The powder X-ray diffraction (XRD) measurements were performed using a Rigaku Miniflex 600, and graphite was used for the peak correction of the XRD profiles (Figure S2c). The Rietveld refinement of the XRD profiles (without graphite) used the GSAS package.[25,26] The cation mixing was refined by the structural model $[Li_{1.05-x}Ni_x]^{3a}[Li_xNi_{0.89-x}Co_{0.10}Mn_{0.01}]^{3b}O_2$ with the space group $R\bar{3}m$, in which Li, transition metal, and O atoms occupy 3a (0, 0, 0.5), 3b (0, 0, 0), and 6c (0, 0, 0.2577) positions, respectively, and a small amount of Li would mix with Ni. Fourier transform infrared (FT-IR) spectroscopy measurements used a Horiba Xplora. Raman spectroscopy measurements used a Horiba Xplora confocal microscopic Raman spectrometer with a laser wavelength of 532 nm. The surface structures of pristine and stored nickel-rich NCM materials were detected using a high-resolution transmission electron microscope (HR-TEM) G2 F30 (Tecnai). The differential scanning calorimetry-thermogravimetry (DSC-TG) curves were collected using a Netzsch 449 F1 Jupiter simultaneous thermal analyzer in a temperature range of 35−850 °C with a heat rate of 5 °C min^{-1}. Contents of surface impurities on pristine and stored nickel-rich NCM materials were measured by a chemical titration method. In detail, 1 g of the material was added into 100 mL of deionized water, stirred for 5 min in a sealed bottle, and filtered to obtain the filtrate. Then, the filtrate was titrated by a calibrated hydrochloric acid solution.

Electrochemical Measurement. The stored nickel-rich NCM material was mixed with acetylene black and poly(vinylidene fluoride) (PVDF) at a mass ratio of 8:1:1, dispersed in *N*-methyl pyrrolidone (NMP), coated on the aluminum foil, then dried at 80 °C overnight in a vacuum oven, and finally punched into wafers to obtain the nickel-rich NCM electrode. The areal loading of the nickel-rich NCM electrode was ~1.90 mg cm^{-2} and its thickness was ~15 μm (Figure S11), which can ensure the homogeneous reaction at the electrode scale and help investigate the intrinsic electrochemical performance caused by the structural degradation of materials. For a CR2016 coin

https://doi.org/10.1021/acssuschemeng.1c02486
ACS Sustainable Chem. Eng. XXXX, XXX, XXX−XXX

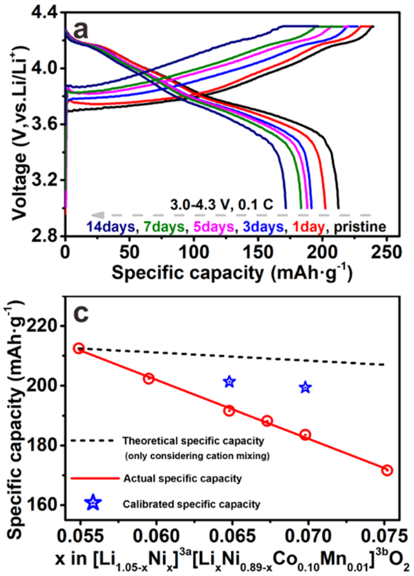

Figure 2. Capacity−voltage curves (a) and the corresponding differential capacity curves (b) of the stored nickel-rich NCM materials in the first cycle at 3.0−4.3 V and 0.1C. The correlation between the first-cycle specific discharge capacity and the Ni content in the lithium layer of the stored nickel-rich NCM materials (c). The cycle performance of the stored nickel-rich NCM materials under different current densities (d).

cell, the nickel-rich NCM electrode was assembled with a Celgard 2400 separator, the commercial electrolyte LB301 (1 M $LiPF_6$ in ethylene carbonate/dimethyl carbonate (EC/DMC), 1:1 by volume), and Li metal in an Ar-filled glovebox. The electrochemical measurements were performed on a LAND CT-2001A battery testing system at 25 °C. For the charging step, the coin cells were constant-current charged to 4.3 V with a current density of 0.1C (1C = 180 $mA\cdot g^{-1}$) and then constant-voltage charged at 4.3 V until the current decreased to 1/10 of the original one. For the discharging step, the coin cells were constant-current discharged to 3.0 V at 0.1C. For the galvanostatic intermittent titration technique (GITT) measurements, the pulse current density was 0.1C and the pulse time was 10 min, followed by a relaxation time of 2 h. The in situ electrochemical impedance spectroscopy (EIS) measurements were performed on an electrochemical workstation Autolab PGSTAT302N (Metrohm, Switzerland) with a frequency range of 100 kHz to 0.1 Hz.

■ RESULTS AND DISCUSSION

The structure, morphology, and element composition of the commercial nickel-rich NCM materials used in this work are confirmed. As shown in Figure S1, the pristine material has the α-$NaFeO_2$ layered structure ($R\bar{3}m$), consisting of spherical secondary particles, and the element composition obtained by ICP-AES is Li/Ni/Co/Mn = 1.05:0.89:0.10:0.01.

The structural evolution of the nickel-rich NCM materials during storage is systematically characterized by XRD, Raman spectroscopy, FT-IR, and DSC-TG measurements, as shown in Figure 1. It is found that the material surface would be gradually coated by the adsorbed species and impurities, accompanied by the formation of a near-surface rock salt structure and the increased cation mixing (Li^+/Ni^{2+}) during storage. First, the XRD patterns in Figures 1a and S2a,b show that the materials maintain a good α-$NaFeO_2$ layered structure before and after storage, belonging to the $R\bar{3}m$ space group.[27,28] However, there still exist three obvious changes in the structure of the stored materials: (i) the appearance of the impurity Li_2CO_3 (Figure 1b); (ii) the shift of the (003) peak position to a lower angle (Figure 1c); and (iii) the decrease in the intensity ratio of the (003) and (104) peaks ($I(003)/I(104)$, Figure S2d). According to previous studies, the shift of the (003) peak position is attributed to the expansion of the c-axis caused by the extraction of Li^+, and the decreased $I(003)/I(104)$ value is closely related to an increased cation mixing in NCM materials.[7,8,29,30] So, these changes in the XRD profile may indicate that the nickel-rich NCM material is gradually delithiated to form the Li_2CO_3 impurity, accompanied by an aggravated cation mixing during storage. The Rietveld refinement of the XRD profiles further confirms the increased cation mixing (Figure S3 and Table S5). The Ni content in the lithium layer (x in $[Li_{1.05-x}Ni_x]^{3a}[Li_xNi_{0.89-x}Co_{0.10}Mn_{0.01}]^{3b}O_2$) gradually increases from 0.0549 Ni to 0.0595 Ni, 0.0648 Ni, 0.0673 Ni, 0.0698 Ni, and 0.0752 Ni after being stored for different times. Second, for the Raman spectroscopy measurement, the new peaks at ∼180 and ∼1095 cm^{-1} in Figure 1d imply the generation of LiOH and Li_2CO_3 on the material surface, respectively.[7,12] In addition, as shown in Figure S4, the relative spectral intensities of the A_{1g} (Ni) and E_g (Ni, Co) peaks decrease with the storage time, indicating a weakened vibration of the $Ni^{3+}O_6$ coordination structure. This may be closely related to the reduction reaction of Ni^{3+}/Ni^{2+}, which tends to aggravate the cation mixing between Li^+ and Ni^{2+} in the structure.[31−34] Third, as for the FT-IR spectra in Figure 1e, the absorption band at 3200−3600 cm^{-1} corresponds to the stretching vibration of O−H, and the absorption peaks at 1496, 1425, and 861 cm^{-1} correspond to the vibration of the CO_3^{2-} group.[10,35] This further confirms the existence of surface impurities (LiOH and Li_2CO_3) on the stored materials. Fourth, as shown in Figure S13a,b and the fast Fourier transform (FFT) image of region 1, the surface of the pristine material has a layered structure belonging to the $R\bar{3}m$ space group. However, in Figure S13c,d and FFT images of regions 2−4, the rock salt structure ($Fm\bar{3}m$ space group) appears in the near-surface region (5−10 nm in thickness) after being stored for 7 days, accompanied by the formation of the surface impurity Li_2CO_3 ($C2/c$ space group). Fifth, through the comparison of DSC-TG curves (Figure 1f−g), besides the mass loss caused by the decomposition of the nickel-rich NCM material beyond 715 °C, there are two additional mass losses

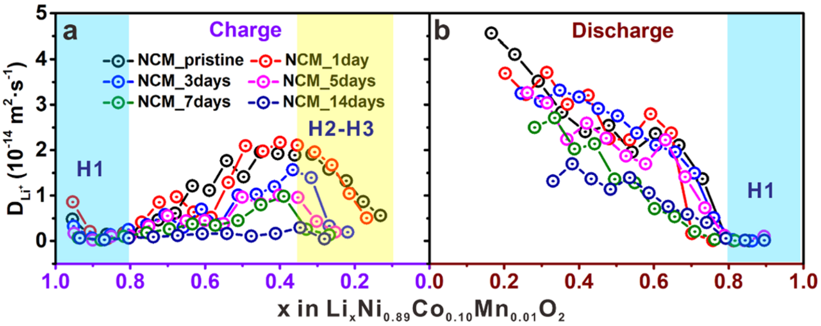

Figure 3. Solid-phase Li^+ diffusion coefficients of the stored nickel-rich NCM materials during the first charging (a) and discharging (b) cycle.

of the stored material: the desorption of the surface-adsorbed species (170−500 °C) and the decomposition of the surface impurities (500−715 °C). It is generally believed that surface-adsorbed species mainly include the adsorbed hydroxyl, bicarbonates, and carbonates formed by the chemical adsorption of H_2O and CO_2 in air.[7,11] Therefore, it can be concluded that the material surface would be gradually coated by adsorbed species (adsorbed hydroxyl, bicarbonates, and carbonates) and impurities (LiOH and Li_2CO_3) during storage. Meanwhile, $Ni^{3+/4+}$ would be reduced to Ni^{2+} with the extraction of Li^+ and the release of the lattice oxygen, thus causing the formation of the near-surface rock salt structure and aggravating the cation mixing in the structure simultaneously. The abovementioned structural evolution of the nickel-rich NCM material during storage is consistent with previous studies.[8,12,19,36] In addition, the contents of surface impurities, which are expressed by the mass fraction of Li (ω_{Li}), are 0.14, 0.36, and 0.48 wt % for the NCM_pristine, NCM_3 days, and NCM_7 days samples, respectively (Table S7).

The basic electrochemical performance of the stored nickel-rich NCM materials is evaluated by charging/discharging the coin cells in a voltage region of 3.0−4.3 V at 0.1C. It is speculated that the Li^+ de/intercalation kinetics may be degraded with the storage time, thereby leading to capacity decay during storage. First, as shown in the capacity−voltage curves of the first charging/discharging cycle (Figure 2a), the nickel-rich NCM materials exhibit an increased charging voltage plateau and a decreased discharging voltage plateau with the storage time, which seriously limits the capacity release. The specific discharge capacity in the first cycle decreases from 212.5 to 202.3, 191.6, 188.2, 183.5, and 171.6 $mAh \cdot g^{-1}$. The detailed electrochemical performance in the first cycle is presented in Table S1. Noting that there exists no significant difference in the first-cycle Coulombic efficiencies of the stored materials. This implies that no electrochemical decomposition of surface impurities has occurred to cause extra irreversibility in a voltage region of 3.0−4.3 V. Actually, this phenomenon is consistent with previous studies, in which the onset potentials of the electrochemical decomposition of LiOH and Li_2CO_3 have been proved to be above 4.3 V (vs Li/Li^+) by both experiments and theoretical calculations.[37−43] Second, the differential capacity curves in Figure 2b show a series of phase transitions (H1−M−H2−H3) that the nickel-rich material undergoes during the charging/discharging process. The increased gap between the oxidation and reduction peak potentials indicates aggravated electrode polarization,[29,44] which conforms to the change in the charging/discharging voltage plateaus in Figure 2a. This may imply a hindered Li^+ kinetics caused by the structural degradation of the stored materials. Noting that a more remarkable change in the shift of the oxidation peak potentials seems to indicate a severer degradation of the Li^+ deintercalation kinetics compared with the Li^+ intercalation kinetics during discharge. Third, Figure 2c presents the correlation between the first-cycle specific discharge capacity and the Ni content in the lithium layer (x in $[Li_{1.05-x}Ni_x]^{3a}[Li_xNi_{0.89-x}Co_{0.10}Mn_{0.01}]^{3b}O_2$) of the stored materials. Generally, the nickel ions mixed into the lithium layer are believed to be electrochemically inert.[21,30] So, the dotted line in Figure 2c shows the theoretical specific discharge capacities of the stored materials (only the irreversible capacity loss caused by the cation mixing is considered, $Q_{theoretical} = 212.5 - \Delta Ni^{3a} \times 273.2$, as shown in the dotted line in Figure 2c). Obviously, there still exists a big gap between the actual specific discharge capacity (the solid line) and the theoretical one. Noting that XRD results can only give the bulk structural information, while the surface layered structure would be partially delithiated to form surface impurities after storage. If all these delithiated layered structures transform into the surface rock salt structure, which is electrochemically inert, the extra irreversible capacity loss can be estimated by the contents of surface impurities in Table S7 ($Q_{loss} = 273.2 \times \Delta\omega_{Li} \times \frac{97.6}{6.9}$). For the NCM_3 days and NCM_7 days samples, these extra capacity losses are approximately 8.5 and 13.1 $mAh \cdot g^{-1}$ respectively, and the calibrated theoretical capacities should be 201.3 and 199.4 $mAh \cdot g^{-1}$ (star symbols in Figure 2c), which are still much larger than their actual capacities. This indicates that the majority of the capacity loss for the stored materials may originate from the degradation of Li^+ de/intercalation kinetics. Fourth, as can be seen from Figure 2d, the capacity gap between different stored materials increases with the current density, further implying the degradation of Li^+ kinetics. If only considering the active lithium loss, the capacity gap between stored materials should be the same theoretically under different current densities. But increasing the current density would magnify the impact of kinetic degradation on capacity, which is like a cask effect. Therefore, we speculate that the Li^+ kinetics may be degraded with the storage time, thus becoming the key factor for the capacity fading of the stored nickel-rich NCM materials.

To confirm the Li^+ kinetic degradation of the stored nickel-rich NCM materials, the solid-phase Li^+ diffusion kinetics inside the materials and the charge transfer kinetics at the electrode/electrolyte interface are systematically investigated by GITT and in situ EIS measurements, respectively. Figure 3 presents the changes in the solid-phase Li^+ diffusion coefficient

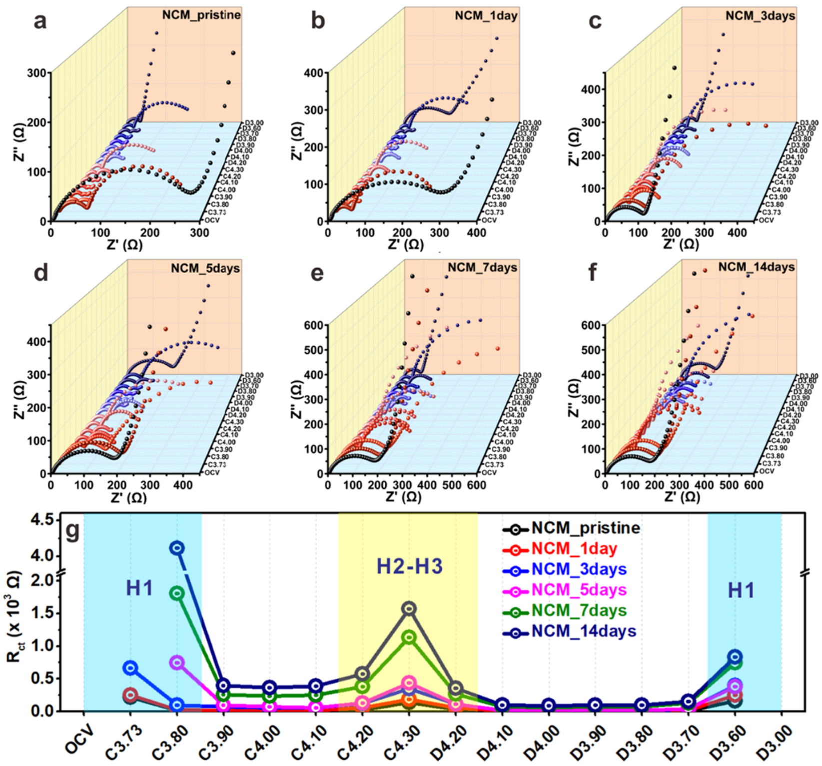

Figure 4. In situ EIS profiles (a−f) and the fitted R_{ct} values (g) of the stored nickel-rich NCM materials during the first charging/discharging cycle.

(D_{Li^+}) of the stored materials during the first charging/discharging cycle. The processing method of the GITT data is shown in Figures S5 and S6. It is found that the solid-phase Li^+ diffusion kinetics would be gradually weakened by the increased cation mixing during storage. First, the D_{Li^+} evolution of the pristine nickel-rich NCM material during the first cycle can be summarized as follows:[29,45−47] (i) At the beginning of charge and the end of discharge ($x > \sim 0.80$ Li), D_{Li^+} is the smallest. It can be attributed to the rare lithium vacancies and narrow space of the lithium layer in the H1 phase. (ii) In the middle of charge (~ 0.35 Li $< x < \sim 0.80$ Li), D_{Li^+} gradually increases with Li^+ deintercalation. This can be related to the increased lithium vacancies and lithium layer space during the phase transition of H1−M−H2. The D_{Li^+} change during the discharging process is just the opposite. (iii) At the end of charge ($x < \sim 0.35$ Li), D_{Li^+} decreases with Li^+ deintercalation. This may be caused by the decreased lithium layer space during the H2−H3 phase transition and the suppression of the Li^+ concentration gradient between the delithiated material and the electrolyte. (iv) At the beginning of discharge ($x < \sim 0.35$ Li), D_{Li^+} is much larger than that at the end of charge, which can be attributed to the acceleration on Li^+ intercalation by the Li^+ concentration gradient. Second, the average D_{Li^+} during the charging/discharging process is found to decrease with the storage time. As shown in Figure S14, surface impurities seem to have no obvious impact on the apparent solid-phase Li^+ diffusion coefficients tested by GITT. So, the decreased D_{Li^+} during storage may be caused by the increased cation mixing in the structure. Specifically, the average D_{Li^+} during the charging/discharging process decreases from 1.04/2.32 × 10^{-14} to 0.12/0.82 × 10^{-14} $m^2 \cdot s^{-1}$ after being stored for 14 days. The detailed D_{Li^+} values of the stored nickel-rich NCM materials are shown in Table S2. Therefore, it can be concluded that the solid-phase Li^+ diffusion kinetics of the H1 phase is the slowest during the charging/discharging process, and the solid-phase Li^+ diffusion kinetics during the charging process is overall slower than that during discharge. Meanwhile, the increased cation mixing can not only lead to an irreversible capacity loss but also weaken the solid-phase Li^+ diffusion kinetics of the nickel-rich NCM materials after storage.

The change in the Li^+ kinetics at the electrode/electrolyte interface after storage is investigated by in situ EIS during the first charging/discharging cycle, as presented in Figure 4a−f. It is found that the adsorbed species, impurities, and rock salt structure formed on the material surface would significantly enhance the interfacial charge transfer resistance (R_{ct}), especially during the first charging process. First, Figure 4a−f shows the in situ EIS spectra of different stored nickel-rich NCM materials. According to previous studies, the high-frequency semicircle that appears at all potentials is mainly associated with the surface film resistance, and the mid-frequency semicircle that appears in some EIS spectra during the charging/discharging cycle is related to the interfacial charge transfer resistance.[36,41] So, in this work, the R_{ct} in each spectrum at different potentials is distinguished as the mid-frequency arc or semicircle. The in situ EIS profiles are fitted using the equivalent circuit diagram in Figure S7. As can be seen from Figure S8, no obvious difference appears in the solution resistance (R_s, the intercept on the real axis at the high-frequency region) and the surface film resistance (R_f, the semicircle in the high-frequency region) between the stored materials.[24,36,48,49] So, emphasis is given to the analysis of the evolution of R_{ct} (the arc or semicircle in the mid-frequency region). Second, Figure 4g and Table S3 show the R_{ct} changes of the stored materials during the first charging/discharging cycle, which mainly exhibit two characteristics: (i) During the charging/discharging process, the R_{ct} in the low-potential region (3.00−3.80 V) and the high-potential region (4.15−4.30 V) is relatively high, corresponding to the H1 phase and the phase transition of H2−H3. (ii) For the pristine material, the R_{ct} value during charge is almost the same as that at the same potential during discharge. However, as the storage time increases, not only the overall R_{ct} values during the charging and discharging processes increase significantly, but also the increase of R_{ct} during charge is much larger than that during discharge. This may be attributed to the surface-adsorbed species, impurities, and rock salt structure formed after storage because the surface-adsorbed species and impurities are believed to be of poor Li^+ conductivity, while the rock salt structure is electrochemically passivated and hard to generate an internal electrical field as the driving force to accelerate the motion of Li^+.[19,24,50] Therefore, it is concluded that the interfacial charge transfer kinetics of the H1 phase is relatively slow. In addition, the surface-adsorbed species, impurities, and rock salt structure would significantly slow down the interfacial charge transfer kinetics of the stored nickel-rich NCM materials, especially during the first charging process.

As confirmed by GITT and in situ EIS measurements, the structural degradation of the nickel-rich NCM material during storage would greatly deteriorate the Li^+ kinetics (both the solid-phase Li^+ diffusion kinetics and the interfacial charge transfer kinetics), especially during the first charging process. This is consistent with the speculation in Figure 2b. To further confirm the correlation between the first-cycle capacity loss and the Li^+ kinetic degradation, the electrochemical tests are performed on the stored nickel-rich NCM materials using the constant-current and constant-voltage charging/discharging steps, as presented in Figure 5. It is found that the degradation of the Li^+ deintercalation kinetics during charge should be responsible for the first-cycle capacity decay during storage in air. First, the capacity during the constant-current charging process gradually decreases with the storage time. As can be seen from the red marks in Figure 5, more and more capacity needs to be released through the constant-voltage charging step, which implies the increased kinetic degradation of Li^+ deintercalation. Second, as shown in the blue marks in Figure 5, the capacity loss after the constant-current discharging step is almost the same (∼0.10 Li) for each material, regardless of the storage time. And it can be restored to a great extent after a constant-voltage discharging step (a potentiostatic hold at 3.0 V for 24 h), which can promote further intercalation of Li^+ into materials. This indicates that this capacity loss seems to be not closely related to the kinetic degradation of Li^+ intercalation during discharge but mainly originates from the intrinsic kinetic limitation of the H1 phase at the end of discharge (Figures 3 and 4g). This is consistent with previous studies.[20,22,23] Noting that the slight difference in overall Coulombic efficiencies of stored materials may be an experimental error. Because the restored capacity during the same hold time should be the same theoretically, but differences between individual half-cells generated during the assembly and operation processes may affect the actual amount of restored capacity as well as the overall Coulombic efficiency. In a word, it is believed that the capacity decay of nickel-rich NCM materials during storage in air is mainly caused by the degradation of Li^+ deintercalation kinetics during charge.

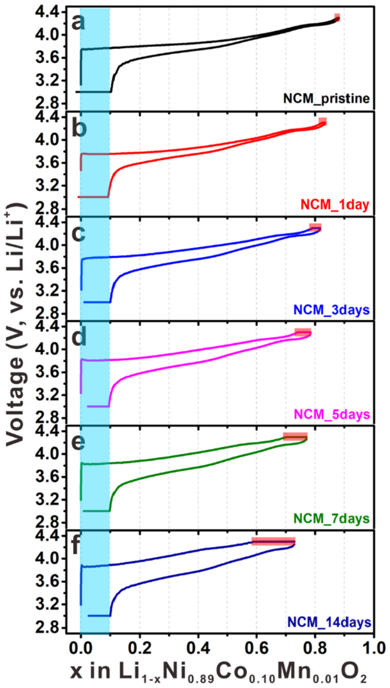

Figure 5. Electrochemical performance of the nickel-rich NCM materials in the first cycle with the constant-current and constant-voltage charging/discharging steps at 3.0−4.3 V (0.1C): the pristine material (a) and materials stored for 1 (b), 3 (c), 5 (d), 7 (e), and 14 (f) days.

As mentioned above, the Li^+ kinetics during the charging process is much slower than that during discharge, thus becoming the key factor in determining the electrochemical performance of the stored nickel-rich NCM materials. On the one hand, owing to the existence of the Li^+ concentration gradient between the delithiated materials and the electrolyte, the solid-phase diffusion of Li^+ intercalation is promoted rather than the Li^+ deintercalation, thus making the solid-phase Li^+ diffusion kinetics during discharge faster than that during charge, as shown in Figure 3. On the other hand, for the Li^+ kinetics at the electrode/electrolyte interface, the kinetic parameters measured by in situ EIS should be the same theoretically at the same potentials during the charging/discharging process because they are unaffected by the Li^+ concentration gradient. However, as shown in Figure 4g, the R_{ct} of the stored materials during the first charging process is much larger than that at the same potential during discharge. To figure out the origin of this difference in R_{ct}, FT-IR and Raman spectroscopy measurements are performed on the pristine and stored materials (signed as NCM_pristine and NCM_14 days), which are soaked in the LB301 electrolyte for 24 h. First, as shown in the FT-IR spectra in Figure 6a,b, the CO_3^{2-} absorption peaks (1496, 1425, and 861 cm^{-1}) of the NCM_14 days sample seem to disappear after being soaked in the electrolyte. The intensity of the absorption band at 3200−3650 cm^{-1} increases obviously, which can be attributed to the stretching vibration of O−H and the vibration of $LiPF_6$.[51,52] In addition, a few absorption peaks appear or strengthen in the range of 800−1500 cm^{-1}: the peaks at 1304 and 848.5 cm^{-1} may correspond to species containing C=O or OCO_2^- (e.g., $ROCO_2Li$), and the peaks at 1265, 929.5, and 890.1 cm^{-1} can be ascribed to the vibration of $Li_xPO_yF_z$ or LiF.[19,51,53,54] However, in Figure 6c, after being rinsed with DMC, the absorption peaks of the electrolyte and new species all disappear and the peaks belonging to LiOH (3200−3600 cm^{-1}) and Li_2CO_3 (1496, 1425, and 861 cm^{-1}) reappear. This

https://doi.org/10.1021/acssuschemeng.1c02486
ACS Sustainable Chem. Eng. XXXX, XXX, XXX−XXX

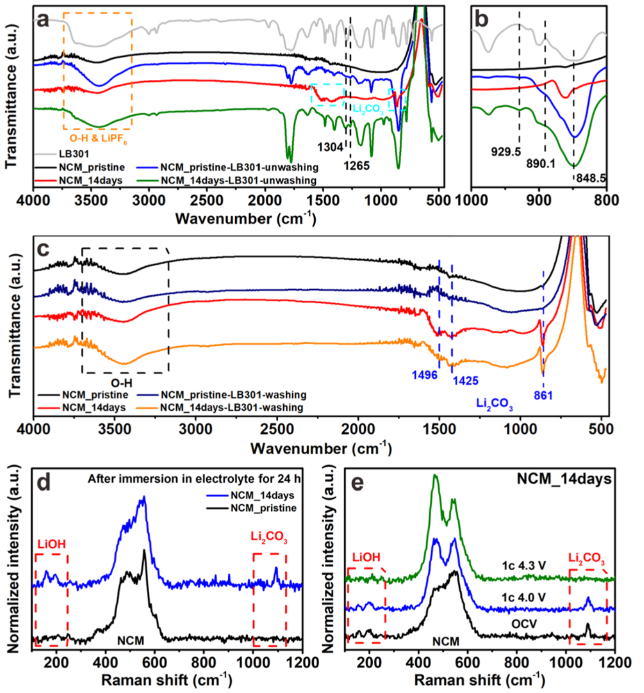

Figure 6. FT-IR spectra of the NCM_pristine and NCM_14 days samples before and after being stored in the electrolyte: without (a, b) or with (c) DMC washing. The Raman spectra of the materials after being stored in the electrolyte without DMC washing (d). The Raman spectra of the NCM_14 days sample after being charged to different potentials in the first cycle (e).

indicates that the surface-adsorbed species may react with the electrolyte to generate new in/organic species (e.g., $ROCO_2Li$, $Li_xPO_yF_z$, and LiF), thus enhancing the R_{ct} during both the charging and discharging processes. But the LiOH and Li_2CO_3 impurities may not participate in the reactions. Second, as can be seen in Figures 6d and S9, Raman spectroscopy measurements also confirm the stability of LiOH and Li_2CO_3 after being stored in the electrolyte. In addition, in Figure 6e, it is found that the surface impurities would disappear only at the end of the first charge (4.0−4.3 V). As discussed in Figure 2a, LiOH and Li_2CO_3 should be electrochemically stable at the working condition in our work. So, the disappearance of the surface impurities in a potential region of 4.0−4.3 V may be caused by the chemical corrosion of the trace HF produced by the parasitic reaction between the nickel-rich NCM material and the electrolyte at high potentials.[54−58] In summary, it is speculated that the decomposition of LiOH and Li_2CO_3 impurities at the end of the first charge (4.0−4.3 V) may be the main reason for the R_{ct} difference between the first charging and discharging processes.

The abovementioned speculation is further verified by in situ EIS and electrochemical charging/discharging tests. First, the in situ EIS measurement is performed on the NCM_14 days sample during the second charging/discharging cycle. In Figure 7a, it is obvious that the R_{ct} values during the second charge are much smaller than those during the first charge, and almost the same as those at the same potentials during discharge. This indicates that the interfacial charge transfer kinetics of the stored material is significantly regenerated after the first charge. Noting that the R_{ct} at 4.3 V in the second cycle is slightly larger than that in the first cycle. On the one hand, the regenerated kinetics during the second charge may make the structure more delithiated, leading to a larger R_{ct} at 4.3 V in turn because the R_{ct} value increases with the delithiation degree at the end of charge (Figure 4g). On the other hand, the gradual deterioration of the surface structure caused by the parasitic reaction between nickel-rich NCM materials and the electrolyte at high potentials may also enhance the R_{ct} value.[24,27] More detailed data are presented in Figure S10 and Table S4. Second, Figure 7b exhibits the cycle performance of the NCM_pristine and NCM_14 days samples in a voltage region of 3.0−4.0/4.3 V. For the NCM_14 days sample, after three cycles at 3.0−4.3 V, the capacity of the subsequent cycles at 3.0−4.0 V is obviously larger than that constantly cycled at 3.0−4.0 V. But there is no significant difference in the capacity for the NCM_pristine sample, which implies the improved Li^+ kinetics of the NCM_14 days sample after the charging process between 4.0 and 4.3 V. Therefore, according to the results in Figure 6, it is concluded that the decomposition of LiOH and Li_2CO_3 impurities at the end of the first charge (4.0−4.3 V) can significantly regenerate the interfacial charge transfer kinetics of the stored materials, making the R_{ct} during the first discharge much smaller than that during the first charge.

■ CONCLUSIONS

In this work, the structure−performance relationship between the structural evolution and the electrochemical performance deterioration of the nickel-rich NCM materials during storage in air is systematically established from the aspect of the Li^+ kinetics. It is found that the Li^+ kinetics (both the solid-phase Li^+ diffusion kinetics and the interfacial charge transfer kinetics) would be significantly weakened by the structural degradation of the stored nickel-rich NCM materials, and the kinetic degradation of Li^+ deintercalation during the charging

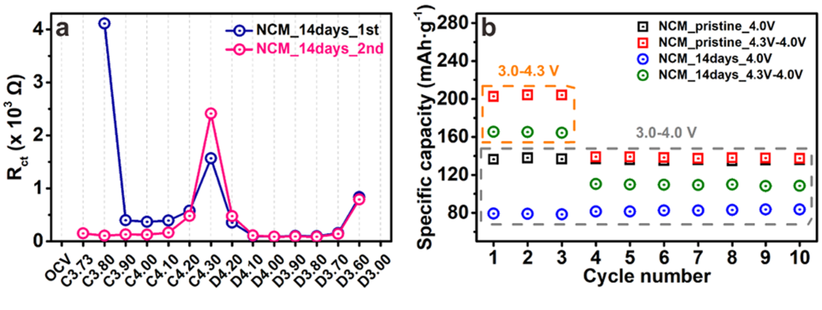

Figure 7. R_{ct} values of the NCM_14 days sample during first and second charging/discharging cycles (a). The cycle performance of the NCM_pristine and NCM_14 days samples at 3.0−4.0/4.3 V (b).

process is the crucial factor for the capacity decay during storage.

First, as revealed by the structural characterization (XRD, FT-IR, Raman spectroscopy, HR-TEM, and DSC-TG), the adsorbed species (the adsorbed hydroxyl, bicarbonates, and carbonates) and impurities (LiOH and Li_2CO_3) would be gradually formed on the material surface, accompanied by the formation of the near-surface rock salt structure and the increased cation mixing (Li^+/Ni^{2+}) in the structure. Second, the GITT and in situ EIS measurements indicate that the increased cation mixing would weaken the solid-phase Li^+ diffusion kinetics, while the surface-adsorbed species, impurities, and rock salt structure would significantly slow down the charge transfer kinetics at the electrode/electrolyte interface. In addition, for the stored nickel-rich NCM materials, the kinetics of Li^+ deintercalation during charge is much slower than that of Li^+ intercalation during discharge, which can be ascribed to the following two reasons: (i) The solid-phase diffusion of Li^+ intercalation would be promoted by the Li^+ concentration gradient between the delithiated material and the electrolyte rather than that of Li^+ deintercalation. (ii) The decomposition of the LiOH and Li_2CO_3 impurities at the end of the first charge cycle (4.0−4.3 V) would greatly regenerate the interfacial charge transfer kinetics for the subsequent charging/discharging processes. Third, through the detailed electrochemical tests, it is found that the degradation of the Li^+ deintercalation kinetics during charge is the dominant factor for the capacity loss of the nickel-rich NCM material during storage in air. Meanwhile, the "irreversible" capacity loss of the first cycle seems to be not closely related to the kinetic degradation of Li^+ intercalation during discharge but mainly originates from the intrinsic kinetic limitation of the H1 phase at the end of discharge.

Through the above systematic research, it can be realized that enhancing the kinetics of Li^+ deintercalation during charge is the key to improve the electrochemical performance of the stored nickel-rich NCM materials. For example, removing the surface impurities by means of alcohol/organic acid washing or the precycle at high cutoff voltages ($\geq$4.3 V), removing the impurities and reducing the cation mixing simultaneously by the secondary calcination, etc. In a word, the results obtained in this work are conducive to deeply understanding the storage performance degradation mechanism of nickel-rich NCM materials and can provide favorable guidance for the modification research.

■ ASSOCIATED CONTENT

SI Supporting Information

The Supporting Information is available free of charge at https://pubs.acs.org/doi/10.1021/acssuschemeng.1c02486.

> XRD, SEM, TEM, and Raman spectra profiles of nickel-rich NCM materials; GITT data and the processing method; in situ EIS profiles and the results of data fitting; electrochemical performances in the first cycle of the stored nickel-rich NCM materials; solid-phase Li^+ diffusion coefficients of water-washed materials; and contents of surface impurities on the stored nickel-rich NCM materials (PDF)

■ AUTHOR INFORMATION

Corresponding Author

Jinbao Zhao − *College of Chemistry and Chemical Engineering, State-Province Joint Engineering Laboratory of Power Source Technology for New Energy Vehicle, State Key Laboratory of Physical Chemistry of Solid Surfaces, Engineering Research Center of Electrochemical Technology, Ministry of Education, Collaborative Innovation Center of Chemistry for Energy Materials, Xiamen University, Xiamen, Fujian 361005, P. R. China;* orcid.org/0000-0002-2753-7508; Phone: +86-05922186935; Email: jbzhao@xmu.edu.cn

Authors

Jiyang Li − *College of Chemistry and Chemical Engineering, State-Province Joint Engineering Laboratory of Power Source Technology for New Energy Vehicle, State Key Laboratory of Physical Chemistry of Solid Surfaces, Engineering Research Center of Electrochemical Technology, Ministry of Education, Collaborative Innovation Center of Chemistry for Energy Materials, Xiamen University, Xiamen, Fujian 361005, P. R. China*

Xin Wang − *College of Chemistry and Chemical Engineering, State-Province Joint Engineering Laboratory of Power Source Technology for New Energy Vehicle, State Key Laboratory of Physical Chemistry of Solid Surfaces, Engineering Research Center of Electrochemical Technology, Ministry of Education, Collaborative Innovation Center of Chemistry for Energy Materials, Xiamen University, Xiamen, Fujian 361005, P. R. China*

Xiangbang Kong − *College of Chemistry and Chemical Engineering, State-Province Joint Engineering Laboratory of Power Source Technology for New Energy Vehicle, State Key Laboratory of Physical Chemistry of Solid Surfaces, Engineering Research Center of Electrochemical Technology, Ministry of Education, Collaborative Innovation Center of Chemistry for Energy Materials, Xiamen University, Xiamen, Fujian 361005, P. R. China*

Huiya Yang − *College of Chemistry and Chemical Engineering, State-Province Joint Engineering Laboratory of Power Source Technology for New Energy Vehicle, State Key Laboratory of Physical Chemistry of Solid Surfaces, Engineering Research Center of Electrochemical Technology, Ministry of Education, Collaborative Innovation Center of Chemistry for Energy Materials, Xiamen University, Xiamen, Fujian 361005, P. R. China*

Jing Zeng − *College of Chemistry and Chemical Engineering, State-Province Joint Engineering Laboratory of Power Source Technology for New Energy Vehicle, State Key Laboratory of Physical Chemistry of Solid Surfaces, Engineering Research Center of Electrochemical Technology, Ministry of Education, Collaborative Innovation Center of Chemistry for Energy Materials, Xiamen University, Xiamen, Fujian 361005, P. R. China*

Complete contact information is available at: https://pubs.acs.org/10.1021/acssuschemeng.1c02486

Notes

The authors declare no competing financial interest.

■ ACKNOWLEDGMENTS

The authors gratefully acknowledge the financial support from the National Key Research and Development Program of China (2017YFB0102000), the National Natural Science Foundation of China (22021001), and the Key Project of Science and Technology of Xiamen (3502Z20201013).

■ REFERENCES

(1) Wang, X.; Ding, Y.-L.; Deng, Y.-P.; Chen, Z. Ni-Rich/Co-Poor Layered Cathode for Automotive Li-Ion Batteries: Promises and Challenges. *Adv. Energy Mater.* **2020**, *10*, No. 1903864.

(2) Chakraborty, A.; Kunnikuruvan, S.; Kumar, S.; Markovsky, B.; Aurbach, D.; Dixit, M.; Major, D. T. Layered Cathode Materials for Lithium-Ion Batteries: Review of Computational Studies on LiNi1−x−yCoxMnyO2 and LiNi1−x−yCoxAlyO2. *Chem. Mater.* **2020**, *32*, 915−952.

(3) Kim, J.; Lee, H.; Cha, H.; Yoon, M.; Park, M.; Cho, J. Prospect and Reality of Ni-Rich Cathode for Commercialization. *Adv. Energy Mater.* **2018**, *8*, No. 1702028.

(4) Liu, B.; Huang, Q.; Su, Y.; Sun, L.; Wu, T.; Wang, G.; Zhang, Q.; Wu, F. Synthesis of Ni-Rich Cathode Material from Maleic Acid-Leachate of Spent Lithium-Ion Batteries. *ACS Sustainable Chem. Eng.* **2020**, *8*, 7839−7850.

(5) Hong-yun, M. A.; Xiao-hui, Y. A.; Meng-yao, M. I.; Yang, Y. I.; Shao-zhong, W. U.; Jiang, Z. H. Degradation Mechanism of LiNi0.83Co0.12Mn0.05O2 Cycled at 45 °C. *J. Electrochem.* **2020**, *26*, 431−440.

(6) Kong, X.; Zhang, Y.; Peng, S.; Zeng, J.; Zhao, J. Superiority of Single-Crystal to Polycrystalline LiNixCoyMn1−x−yO2 Cathode Materials in Storage Behaviors for Lithium-Ion Batteries. *ACS Sustainable Chem. Eng.* **2020**, *8*, 14938−14948.

(7) Chen, Z.; Wang, J.; Huang, J.; Fu, T.; Sun, G.; Lai, S.; Zhou, R.; Li, K.; Zhao, J. The High-Temperature and High-Humidity Storage Behaviors and Electrochemical Degradation Mechanism of LiNi0.6-Co0.2Mn0.2O2 Cathode Material for Lithium Ion Batteries. *J. Power Sources* **2017**, *363*, 168−176.

(8) Kong, X.; Peng, S.; Li, J.; Chen, Z.; Chen, Z.; Wang, J.; Zhao, J. Pre-Blended Conductive Agent to Effectively Improve the Storage Properties of LiNi0.6Co0.2Mn0.2O2 Cathode Materials. *J. Power Sources* **2020**, *448*, No. 227445.

(9) Matsumoto, K.; Kuzuo, R.; Takeya, K.; Yamanaka, A. Effects of CO2 in Air on Li Deintercalation from LiNi1-x-yCoxAlyO2. *J. Power Sources* **1999**, *81*−*82*, 558−561.

(10) Zhuang, G. V.; Chen, G.; Shim, J.; Song, X.; Ross, P. N.; Richardson, T. J. Li2CO3 in LiNi0.8Co0.15Al0.05O2 Cathodes and its Effects on Capacity and Power. *J. Power Sources* **2004**, *134*, 293−297.

(11) Liu, H.; Yang, Y.; Zhang, J. Investigation and Improvement on the Storage Property of LiNi0.8Co0.2O2 as a Cathode Material for Lithium-Ion Batteries. *J. Power Sources* **2006**, *162*, 644−650.

(12) Zhang, X.; Jiang, W. J.; Zhu, X. P.; Mauger, A.; Lu, Q.; Julien, C. M. Aging of LiNi1/3Mn1/3Co1/3O2 Cathode Material upon Exposure to H2O. *J. Power Sources* **2011**, *196*, 5102−5108.

(13) Huang, B.; Qian, K.; Liu, Y.; Liu, D.; Zhou, K.; Kang, F.; Li, B. Investigations on the Surface Degradation of LiNi1/3Co1/3Mn1/3O2 after Storage. *ACS Sustainable Chem. Eng.* **2019**, *7*, 7378−7385.

(14) Liu, H. S.; Zhang, Z. R.; Gong, Z. L.; Yang, Y. Origin of Deterioration for LiNiO2 Cathode Material during Storage in Air. *Electrochem. Solid-State Lett.* **2004**, *7*, A190−A193.

(15) Lv, C.; Li, Z.; Ren, X.; Li, K.; Ma, J.; Duan, X. Revealing the Degradation Mechanism of Ni-Rich Cathode Materials after Ambient Storage and Related Regeneration Method. *J. Mater. Chem. A* **2021**, *9*, 3995−4006.

(16) Sicklinger, J.; Metzger, M.; Beyer, H.; Pritzl, D.; Gasteiger, H. A. Ambient Storage Derived Surface Contamination of NCM811 and NCM111: Performance Implications and Mitigation Strategies. *J. Electrochem. Soc.* **2019**, *166*, A2322−A2335.

(17) Jung, R.; Morasch, R.; Karayaylali, P.; Phillips, K.; Maglia, F.; Stinner, C.; Shao-Horn, Y.; Gasteiger, H. A. Effect of Ambient Storage on the Degradation of Ni-Rich Positive Electrode Materials (NMC811) for Li-Ion Batteries. *J. Electrochem. Soc.* **2018**, *165*, A132−A141.

(18) Grenier, A.; Liu, H.; Wiaderek, K. M.; Lebens-Higgins, Z. W.; Borkiewicz, O. J.; Piper, L. F. J.; Chupas, P. J.; Chapman, K. W. Reaction Heterogeneity in LiNi0.8Co0.15Al0.05O2 Induced by Surface Layer. *Chem. Mater.* **2017**, *29*, 7345−7352.

(19) Chen, Z.; Liu, C.; Sun, G.; Kong, X.; Lai, S.; Li, J.; Zhou, R.; Wang, J.; Zhao, J. Electrochemical Degradation Mechanism and Thermal Behaviors of the Stored LiNi0.5Co0.2Mn0.3O2 Cathode Materials. *ACS Appl. Mater. Interfaces* **2018**, *10*, 25454−25464.

(20) Grenier, A.; Reeves, P. J.; Liu, H.; Seymour, I. D.; Märker, K.; Wiaderek, K. M.; Chupas, P. J.; Grey, C. P.; Chapman, K. W. Intrinsic Kinetic Limitations in Substituted Lithium-Layered Transition-Metal Oxide Electrodes. *J. Am. Chem. Soc.* **2020**, *142*, 7001−7011.

(21) Makimura, Y.; Sasaki, T.; Nonaka, T.; Nishimura, Y. F.; Uyama, T.; Okuda, C.; Itou, Y.; Takeuchi, Y. Factors affecting cycling life of LiNi0.8Co0.15Al0.05O2 for lithium-ion batteries. *J. Mater. Chem. A* **2016**, *4*, 8350−8358.

(22) Kasnatscheew, J.; Evertz, M.; Streipert, B.; Wagner, R.; Klöpsch, R.; Vortmann, B.; Hahn, H.; Nowak, S.; Amereller, M.; Gentschev, A.-C.; Lamp, P.; Winter, M. The Truth about the 1st Cycle Coulombic Efficiency of LiNi1/3Co1/3Mn1/3O2 (NCM) Cathodes. *Phys. Chem. Chem. Phys.* **2016**, *18*, 3956−3965.

(23) Robert, R.; Novák, P. Switch of the Charge Storage Mechanism of LixNi0.80Co0.15Al0.05O2 at Overdischarge Conditions. *Chem. Mater.* **2018**, *30*, 1907−1911.

(24) Li, J.; Huang, J.; Kong, X.; Zeng, J.; Zhao, J. The Apparent Capacity Decay by Kinetic Degradation of LiNi0.5Co0.2Mn0.3O2 during Cycling under the High Upper-Limit Charging Potential. *J. Power Sources* **2021**, *496*, No. 229856.

(25) Larson, A. C.; Von Dreele, R. B. *Report LAUR 86-748*; Los Alamos National Laboratory: New Mexico, USA, 1986−2004.

(26) Toby, B. H. EXPGUI, a Graphical User Interface for GSAS. *J. Appl. Crystallogr.* **2001**, *34*, 210−213.

(27) Jung, S.-K.; Gwon, H.; Hong, J.; Park, K.-Y.; Seo, D.-H.; Kim, H.; Hyun, J.; Yang, W.; Kang, K. Understanding the Degradation Mechanisms of LiNi0.5Co0.2Mn0.3O2 Cathode Material in Lithium Ion Batteries. *Adv. Energy Mater.* **2014**, *4*, No. 1300787.

(28) Lee, S.; Jang, D.; Yoon, J.; Cho, Y.-H.; Lee, Y.-S.; Kim, D.-H.; Kim, W.-S.; Yoon, W.-S. Crystal Structure Changes of LiNi0.5-Co0.2Mn0.3O2 Cathode Materials During the First Charge Investigated by in situ XRD. *J. Electrochem. Sci. Technol.* **2012**, *3*, 29−34.

(29) Noh, H.-J.; Youn, S.; Yoon, C. S.; Sun, Y.-K. Comparison of the Structural and Electrochemical Properties of Layered Li-[NixCoyMnz]O2 (x = 1/3, 0.5, 0.6, 0.7, 0.8 and 0.85) Cathode Material for Lithium-Ion Batteries. *J. Power Sources* **2013**, *233*, 121−130.

(30) Zhang, M.-J.; Teng, G.; Chen-Wiegart, Y.-c. K.; Duan, Y.; Ko, J. Y. P.; Zheng, J.; Thieme, J.; Dooryhee, E.; Chen, Z.; Bai, J.; Amine, K.; Pan, F.; Wang, F. Cationic Ordering Coupled to Reconstruction of Basic Building Units during Synthesis of High-Ni Layered Oxides. *J. Am. Chem. Soc.* **2018**, *140*, 12484−12492.

(31) Julien, C. Local Cationic Environment in Lithium Nickel−Cobalt Oxides Used as Cathode Materials for Lithium Batteries. *Solid State Ion.* **2000**, *136*−*137*, 887−896.

(32) Nanda, J.; Remillard, J.; O'Neill, A.; Bernardi, D.; Ro, T.; Nietering, K. E.; Go, J.-Y.; Miller, T. J. Local State-of-Charge Mapping of Lithium-Ion Battery Electrodes. *Adv. Funct. Mater.* **2011**, *21*, 3282−3290.

(33) Ghanty, C.; Markovsky, B.; Erickson, E. M.; Talianker, M.; Haik, O.; Tal-Yossef, Y.; Mor, A.; Aurbach, D.; Lampert, J.; Volkov, A.; Shin, J.-Y.; Garsuch, A.; Chesneau, F. F.; Erk, C. Li+-Ion Extraction/Insertion of Ni-Rich Li1+x(NiyCozMnz)wO2 (0.005 < x < 0.03; y:z = 8:1, w=1) Electrodes: In Situ XRD and Raman Spectroscopy Study. *ChemElectroChem* **2015**, *2*, 1479−1486.

https://doi.org/10.1021/acssuschemeng.1c02486

(34) Flores, E.; Novák, P.; Aschauer, U.; Berg, E. J. Cation Ordering and Redox Chemistry of Layered Ni-Rich LixNi1−2yCoyMnyO2: An Operando Raman Spectroscopy Study. *Chem. Mater.* **2019**, *32*, 186−194.

(35) Xiong, X.; Wang, Z.; Yue, P.; Guo, H.; Wu, F.; Wang, J.; Li, X. Washing Effects on Electrochemical Performance and Storage Characteristics of LiNi0.8Co0.1Mn0.1O2 as Cathode Material for Lithium-Ion Batteries. *J. Power Sources* **2013**, *222*, 318−325.

(36) Zhao, X.; Zhuang, Q.-C.; Wu, C.; Wu, K.; Xu, J.-M.; Zhang, M.-Y.; Sun, X.-L. Impedance Studies on the Capacity Fading Mechanism of Li(Ni0.5Co0.2Mn0.3)O2 Cathode with High-Voltage and High-Temperature. *J. Electrochem. Soc.* **2015**, *162*, A2770−A2779.

(37) Ling, C.; Zhang, R.; Takechi, K.; Mizuno, F. Intrinsic Barrier to Electrochemically Decompose Li2CO3 and LiOH. *J. Phys. Chem. C* **2014**, *118*, 26591−26598.

(38) Meini, S.; Tsiouvaras, N.; Schwenke, K. U.; Piana, M.; Beyer, H.; Lange, L.; Gasteiger, H. A. Rechargeability of Li−Air Cathodes Pre-Filled with Discharge Products Using an Ether-Based Electrolyte Solution: Implications for Cycle-Life of Li−Air Cell. *Phys. Chem. Chem. Phys.* **2013**, *15*, 11478−11493.

(39) Wang, R.; Yu, X.; Bai, J.; Li, H.; Huang, X.; Chen, L.; Yang, X. Electrochemical Decomposition of Li2CO3 in NiO-Li2CO3 Nanocomposite Thin Film and Powder Electrodes. *J. Power Sources* **2012**, *218*, 113−118.

(40) Freunberger, S. A.; Chen, Y.; Peng, Z.; Griffin, J. M.; Hardwick, L. J.; Barde, F.; Novak, P.; Bruce, P. G. Reactions in the Rechargeable Lithium-O2 Battery with Alkyl Carbonate Electrolytes. *J. Am. Chem. Soc.* **2011**, *133*, 8040−8047.

(41) Robert, R.; Bünzli, C.; Berg, E. J.; Novák, P. Activation Mechanism of LiNi0.80Co0.15Al0.05O2: Surface and Bulk Operando Electrochemical, Differential Electrochemical Mass Spectrometry, and X-ray Diffraction Analyses. *Chem. Mater.* **2015**, *27*, 526−536.

(42) Bi, Y.; Wang, T.; Liu, M.; Du, R.; Yang, W.; Liu, Z.; Peng, Z.; Liu, Y.; Wang, D.; Sun, X. Stability of Li2CO3 in Cathode of Lithium Ion Battery and its Influence on Electrochemical Performance. *RSC Adv.* **2016**, *6*, 19233−19237.

(43) Renfrew, S. E.; McCloskey, B. D. Residual Lithium Carbonate Predominantly Accounts for First Cycle CO2 and CO Outgassing of Li-Stoichiometric and Li-Rich Layered Transition-Metal Oxides. *J. Am. Chem. Soc.* **2017**, *139*, 17853−17860.

(44) Han, Y.; Heng, S.; Wang, Y.; Qu, Q.; Zheng, H. Anchoring Interfacial Nickel Cations on Single Crystal LiNi0.8Co0.1Mn0.1O2 Cathode Surface via Controllable Electron Transfer. *ACS Energy Lett.* **2020**, *5*, 2421−2433.

(45) Hong, C.; Leng, Q.; Zhu, J.; Zheng, S.; He, H.; Li, Y.; Liu, R.; Wan, J.; Yang, Y. Revealing the Correlation between Structural Evolution and Li+ Diffusion Kinetics of Nickel-Rich Cathode Materials in Li-Ion Batteries. *J. Mater. Chem. A* **2020**, *8*, 8540−8547.

(46) Märker, K.; Reeves, P. J.; Xu, C.; Griffith, K. J.; Grey, C. P. Evolution of Structure and Lithium Dynamics in LiNi0.8Mn0.1Co0.1O2 (NMC811) Cathodes during Electrochemical Cycling. *Chem. Mater.* **2019**, *31*, 2545−2554.

(47) Zhou, H.; Xin, F.; Pei, B.; Whittingham, M. S. What Limits the Capacity of Layered Oxide Cathodes in Lithium Batteries? *ACS Energy Lett.* **2019**, *4*, 1902−1906.

(48) Laszczynski, N.; Solchenbach, S.; Gasteiger, H. A.; Lucht, B. L. Understanding Electrolyte Decomposition of Graphite/NCM811 Cells at Elevated Operating Voltage. *J. Electrochem. Soc.* **2019**, *166*, A1853−A1859.

(49) Yan, P.; Sun, X.; Zheng, J.; Wang, C.; Liu, J.; Wang, B.; Cheng, X.; Zhang, J.-G. Tailoring Grain Boundary Structures and Chemistry of Ni-Rich Layered Cathodes for Enhanced Cycle Stability of Lithium-Ion Batteries. *Nat. Energy* **2018**, *3*, 600−605.

(50) Song, S. H.; Cho, M.; Park, I.; Yoo, J.-G.; Ko, K.-T.; Hong, J.; Kim, J.; Jung, S.-K.; Avdeev, M.; Ji, S.; Lee, S.; Bang, J.; Kim, H. High-Voltage-Driven Surface Structuring and Electrochemical Stabilization of Ni-Rich Layered Cathode Materials for Li Rechargeable Batteries. *Adv. Energy Mater.* **2020**, *10*, No. 2000521.

(51) Aurbach, D.; Gamolsky, K.; Markovsky, B.; Salitra, G.; Gofer, Y.; Heider, U.; Oesten, R.; Schmidt, M. The Study of Surface Phenomena Related to Electrochemical Lithium Intercalation into LixMOy Host Materials (M = Ni, Mn). *J. Electrochem. Soc.* **2000**, *147*, 1322−1331.

(52) Ostrovskii, D.; Ronci, F.; Scrosati, B.; Jacobsson, P. Reactivity of Lithium Battery Electrode Materials toward Non-Aqueous Electrolytes: Spontaneous Reactions at the Electrode−Electrolyte Interface Investigated by FTIR. *J. Power Sources* **2001**, *103*, 10−17.

(53) Ostrovskii, D.; Ronci, F.; Scrosati, B.; Jacobsson, P. A FTIR and Raman Study of Spontaneous Reactions Occurring at the LiNiyCo1-yO2 Electrode/Non-Aqueous Electrolyte Interface. *J. Power Sources* **2001**, *94*, 183−188.

(54) Yu, Y.; Pinar, K.; Yu, K.; Livia, G.; Magali, G.; Filippo, M.; Roland, J.; Isaac, L.; Yang, S.-H. Coupled LiPF6 Decomposition and Carbonate Dehydrogenation Enhanced by Highly Covalent Metal Oxides in High-Energy Li-Ion Batteries. *J. Phys. Chem. C* **2018**, *122*, 27368−27382.

(55) Zhou, R.; Huang, J.; Lai, S.; Li, J.; Wang, F.; Chen, Z.; Lin, W.; Li, C.; Wang, J.; Zhao, J. A Bifunctional Electrolyte Additive for H2O/HF Scavenging and Enhanced Graphite/ LiNi0.5Co0.2Mn0.3O2 Cell Performance at a High Voltage. *Sustainable Energy Fuels* **2018**, *2*, 1481−1490.

(56) Ravdel, B.; Abraham, K. M.; Gitzendanner, R.; DiCarlo, J.; Lucht, B.; Campion, C. Thermal Stability of Lithium-Ion Battery Electrolytes. *J. Power Sources* **2003**, *119−121*, 805−810.

(57) Campion, C. L.; Li, W.; Lucht, B. L. Thermal Decomposition of LiPF6-Based Electrolytes for Lithium-Ion Batteries. *J. Electrochem. Soc.* **2005**, *152*, A2327−A2334.

(58) Zhang, Y.; Katayama, Y.; Tatara, R.; Giordano, L.; Yu, Y.; Fraggedakis, D.; Sun, J. G.; Maglia, F.; Jung, R.; Bazant, M. Z.; Shao-Horn, Y. Revealing Electrolyte Oxidation via Carbonate Dehydrogenation on Ni-Based Oxides in Li-Ion Batteries by In Situ Fourier Transform Infrared Spectroscopy. *Energy Environ. Sci.* **2020**, *13*, 183−199.